CHALMERS
UNIVERSITY OF TECHNOLOGY

Cu precipitation in electron-irradiated iron alloys for spent-fuel canisters

Journal of Nuclear Materials 572 (2022) 154038

Contents lists available at ScienceDirect

Journal of Nuclear Materials

journal homepage: www.elsevier.com/locate/jnucmat

Cu precipitation in electron-irradiated iron alloys for spent-fuel canisters

Qigui Yang[a], Zhongwen Chang[b], Luca Messina[c], Nils Sandberg[d], Nicolas Castin[e], Amine Yousfi[f], Elin Toijer[a], Mattias Thuvander[g], Bruno Boizot[h], Vincent Metayer[i], Dominique Gorse-Pomonti[j], Pär Olsson[a,*]

[a] Nuclear Engineering, KTH Royal Institute of Technology, Roslagstullsbacken 21, Stockholm 114 21, Sweden
[b] Reactor Core and Fuel Department, Forsmarks Kraftgrupp AB, Östhammar 742 03, Sweden
[c] CEA, DEs, DEC, IRESNE, Cadarache, Saint-Paul-Lez-Durance F-13108, France
[d] Swedish Radiation Safety Authority, Solna Strandväg 96, Stockholm SE-171 16, Sweden
[e] Institute of Nuclear Materials Science, Belgian Nuclear Research Centre, Boeretang 200, Mol 2400, Belgium
[f] RISE Research Institute of Sweden, Mölndal SE-43153, Sweden
[g] Department of Physics, Chalmers University of Technology, Göteborg SE-412 96, Sweden
[h] CEA, Service de Recherches de Métallurgie Physique, Gif-sur Yvette, Cedex 91191, France
[i] CEA, Grand Accélérateur National d'Ions Lourds, Boulevard Henri Becquerel, Caen, Cedex, France
[j] Laboratoire des Solides Irradiés, CNRS, Ecole Polytechnique, CEA/DRF/IRAMIS, Palaiseau F-91128, France

ARTICLE INFO

Article history:
Received 25 February 2022
Revised 15 August 2022
Accepted 13 September 2022
Available online 14 September 2022

ABSTRACT

In this work, the Cu clustering in Fe under irradiation is investigated using experiments, cluster dynamics and atomistic kinetic Monte Carlo (AKMC) simulations. In experiments, cast iron and model FeCu alloy samples were irradiated with 2 MeV electrons for 143 h at 140 °C. The post-irradiation microstructure was characterized using atom probe tomography. Cluster dynamics and AKMC methods were used to simulate the Cu clustering under the same irradiation conditions. Both simulation methods show satisfactory agreement with experiments, lending strength to the validity of the models. Finally, the Cu clustering in spent-fuel repository conditions for 10^5 years at 100 °C was simulated using both methods. The results indicate that potential hardening by Cu clustering is insignificant over 10^5 years.

1. Introduction

The current design of canisters for the spent-fuel final repository in Sweden considers the use of a load-bearing cast iron insert surrounded by a tight copper shell. Copper is meant to protect the canister against corrosion in the repository underground environment, whereas the cast-iron insert provides the mechanical strength to bear the external stresses the canister might be exposed to during its hundreds of thousand-year long task. It is necessary to ensure that the mechanical strength is maintained, so that any loss of radioactive substances to the environment is prevented. One of the possible threats might come from the effects of the radiation emitted by spent fuel. Cast iron can contain low but non-negligible amounts of Cu and it is well known from neutron irradiation in reactor pressure vessel (RPV) steels that a weakly supersaturated Cu content is sufficient for the formation of small Cu-rich nano-precipitates, which in turn are responsible for hardening and a ductile-to-brittle transition temperature (DBTT) shift [1]. In the canisters, a weak but non-negligible flux of Frenkel pairs (FP) is produced by high-energy electrons that are generated through Compton scattering induced by the spent-fuel gamma radiation. In any ordinary application, weakly supersaturated alloys and very weak radiation fluxes would not lead to any significant changes in mechanical properties, but for the spent fuel canisters the total lifetime is so long that one cannot dismiss the potential damaging effects off hand. The canister integrity in the long-time perspective can be affected by the spent fuel radiation and is a potential risk that needs to be properly assessed.

Irradiation-enhanced and induced precipitation of Cu in Fe has been extensively studied for RPV steels, both experimentally and on the modeling side (see [2–6] for a review). However, the difference in temperature between RPV operation (300 °C) and the repository environment (about 100 °C for the first few hundred years, slowly decreasing towards the bedrock temperature) hampers the transferability of those studies to the canister case. The

* Corresponding author.
E-mail address: polsson@kth.se (P. Olsson).

https://doi.org/10.1016/j.jnucmat.2022.154038

difference in temperature has the significant effect of slowing down diffusion drastically but at the same time leads to stronger driving force for Cu precipitation due to the enhanced supersaturation. Some theoretical studies were specifically devoted to this issue. In Ref. [7], the damage rate on the canister wall was found to be excessively small for any mechanical property change to be visible. However, in this work the possibility of Cu precipitation was completely disregarded. Later, Brissoneau et al. [8] calculated damage rates based on typical spent fuels, and predicted the formation of Cu precipitates in the first few years of storage, suggesting a predicted maximum limit of 0.05 at.% Cu to avoid the embrittlement effect. A more recent cluster dynamics study [9] confirmed the formation of small but diffuse Cu nanoprecipitates, showing that the onset of precipitation in the model is very sensitive to the low-temperature Cu diffusivity in iron, a parameter that is difficult to assess accurately.

The Cu-content threshold of 0.05 at.% suggested by Ref. [8] should be taken, consequently, as an indication of a potential risk where further supporting experiments and modeling studies are needed. Notably, two strong limitations need to be addressed. Firstly, Cu diffusion data are extrapolated from high-temperature measurements, and the obtained Cu diffusion coefficient is in strong disagreement with recent low-temperature studies [10,11]. Furthermore, the gamma energy of the main emitter (Cs-137) produces Compton electrons that can maximally transfer just below the average displacement threshold in pure iron; however, the model in [8] does not account in a clear way for the possibility of sub-threshold displacements, which are possible in some preferential lattice directions [12].

The aim of this work is therefore to compensate for the lack of experimental data on Cu precipitation in the canister insert, by performing specific electron-irradiation experiments on cast iron and a Fe-Cu model alloy. The experimental results are then supported by a thorough modeling of Cu precipitation kinetics at low temperatures, where the sensitive parameters (Cu diffusivity and sub-threshold displacements) are carefully assessed. Electron irradiation is chosen because it produces single Frenkel pairs (FPs) and thus mimics well the effect of gamma radiation on the canister material. With respect to the repository conditions, in the experiment the Cu precipitation kinetics is accelerated by both inducing a higher defect population, and by slightly raising the irradiation temperature (140 °C), to accelerate the diffusion while inducing only minimal changes in the alloy thermodynamic and magnetic properties.

The experiments are modeled with a combination of cluster dynamics and atomistic kinetic Monte Carlo (AKMC) simulations. Firstly, the experimental damage rate is carefully assessed with the PIEDMONT code [13]. This Monte Carlo code is developed specifically for electron-irradiation experiments on metallic samples. It provides a precise estimation of total damage rates and spatial damage profiles in displacement-per-atom (dpa) units. It also includes an improved formulation of the damage model that considers the possibility for sub-threshold displacements [14].

Finally, cluster dynamics and AKMC simulations are used to calculate the cluster size distribution of Cu atoms in iron under different irradiation conditions. The simulation results contain both the model validation on the experimental results, and the simulation of real repository conditions.

2. Experimental details

The experiments were performed at the SIRIUS electron irradiation facility at the Irradiated Solids Laboratory in Palaiseau, France. It is a high-energy electron Pelletron accelerator from NEC. In order to obtain a stable irradiation temperature of 140 °C, a current of 20 μA, at an electron kinetic energy of 2 MeV, was used for the irradiation. The samples were irradiated for 143 h.

Table 1
Nominal composition of the materials used in the irradiation experiment.

Element (at.%)	Cast iron	FeCu alloy
Cu	0.028	0.079
Mn	0.141	0.01
Ni	0.329	< 0.005
C	14.6	< 0.01
P	0.039	0.011
Si	3.96	0.01
Fe	balance	balance

The irradiation was performed on two different alloys: a model FeCu alloy ($\approx$ 0.08 at.% Cu) sample, obtained from the REVE project [15], and three cast-iron samples ($\approx$ 0.03 at.% Cu) taken from insert I53 from Svensk Kärnbränslehantering AB (SKB). The nominal compositions are shown in Table 1. From the atom probe tomography (APT) analysis, the FeCu alloy had 0.082 at.% Cu and 0.079 at.% Cu, in the samples before and after irradiation, respectively. The APT analysis of the cast iron samples was very challenging and only one tip gave any useful statistics. From this sample, the measured composition was 0.007 at.% Cu, which is lower than the nominal one. The difference in absolute terms is understandable from the small samples size. Besides the difference in Cu content, it is worth noticing the difference in C and Si composition between the two alloys. All samples were identical in dimensions ($16 \times 4 \times 2$ mm^3) and were mounted during irradiation in the same beam line.

The post-irradiation microstructure was then characterized by APT using a wide-angle local electrode atom probe (Imago LEAP 3000X HR), with a detection efficiency of 37%, at Chalmers University of Technology, Sweden. The analysis of the model FeCu alloy, carried out as well on non-irradiated reference samples, was performed in voltage-pulse mode with a pulse fraction of 20% and a pulse frequency of 200 kHz. The sample temperature was 70 K, and the DC voltage was regulated to keep an evaporation rate of 0.5% (ions/pulse). The cast iron was analyzed in laser-pulse mode (pulse energy 0.3 nJ, temperature 50 K, pulse frequency 200 kHz and evaporation rate 0.5%), as several attempts of using voltage-pulsing gave no useful data.

The APT data was evaluated using the software IVAS 3.4/3.6. The reconstructions were made using the voltage method. For the model FeCu alloy analyses the reconstructions were calibrated using the (200) and the (110) poles in the detector hit maps and the corresponding interplanar spacings, using an evaporation field of 33 V/nm. For the short cast iron analysis, poles could not be identified, so the reconstruction was made using default parameters, and a field of 25 V/nm. In addition to atom maps, the copper distribution was analyzed using the radial distribution function (RDF), the nearest-neighbor distance distribution (NNDD) and the clustering algorithm maximum separation method (MSM) [16]. The RDF is constructed as the bulk-concentration normalized average of the radial concentration profiles centered on each Cu atom. If there is clustering, the concentration (or the relative concentration) will be high at very short distances. The NNDD plots the distribution of distances between Cu-Cu nearest neighbors, and the results are compared with the same distribution calculated from a randomized dataset (with the same atom positions as in the experimental dataset, but with the atom identities exchanged at random). A tendency to clustering is found if the experimental NNDD is shifted towards shorter distances compared with the randomized NNDD. The MSM algorithm, incorporated in the IVAS software, corresponds to the standard algorithm for clustering analysis [16]. However, it should be noted that as there is no strict cluster defini-

tion, the choice of the algorithm parameters is somewhat arbitrary. In the present study, the parameters were chosen as $d_{max} = 1.2$ nm and $N_{min} = 5$, where d_{max} is the maximum separation parameter (i.e., atoms closer than this distance are considered as a part of the same cluster), and N_{min} is the minimum number of atoms to be considered as clusters.

3. Modelling details

3.1. Dose estimation

The model validation of experiments requires a proper calculation of the damage dose and dose rate. The total dose was distributed on four samples.

The damage dose rate is estimated by PIEDMONT, a random walk-based Monte Carlo code that simulates the propagation of electrons in metals by a sequence of electron-nucleus elastic interactions, and allows for an accurate computation of the damage rate. A detailed description of the code can be found in [13]. In iron, the average threshold displacement energy (TDE) is 32 eV based on *ab initio* molecular dynamics (MD) calculations [12], and the scattering cross section for 2 MeV electrons is 50 barn [17]. Following the NRT dpa formula [18], this yields an approximate dose of 7.0×10^{-4} dpa. For a total irradiation time of 143 h, the resulting irradiation rate is 1.37×10^{-9} dpa/s. However, there are well-known overestimation issues with estimating the damage rate using the NRT model [14,19]. Recent *ab initio* molecular dynamics calculations [12] have also shown a strong angular anisotropy. This means that the displacement probability at each collision varies in a continuous manner between 0 and 1 across a relatively wide energy range, from approximately 18 to 65 eV. The predicted minimum of 18 eV [12] is consistent with previous experimental evidences [20,21]. In order to account for this sub-threshold displacement probability, a full energy range primary damage model [14] is included in the PIEDMONT code.

This full energy range model [14] is of particular importance to apply for radiation-matter interactions where the energy transfer is near the TDE. This is the case for the canister cast iron exposed to the spent-fuel gamma radiation. For example, the Compton electrons created by the gamma rays of the main emitter (Cs-137) can provide a maximal energy transfer to the primary knock-out atoms of about 27 eV, which is below the theoretical average TDE value of 32 eV and well below the standard average TDE literature value of 40 eV [22]. Thus, even though according to the traditional displacement models [18,23] and to the more recent athermal recombination corrected model [19] there should be no damage, the possibility of sub-threshold displacements below 32 eV is crucial and needs to be carefully evaluated, especially considered that even a small amount of damage can accumulate to large quantities over the expected fuel-canister life span. Under the experimental irradiation conditions (2 MeV electrons), the PIEDMONT code with the aforementioned modified damage model [14] yields a total dose of 9.3×10^{-4} dpa and a corresponding dose rate of 1.81×10^{-9} dpa/s, hence about 30% higher than the simplified estimation (1.37×10^{-9} dpa/s). This corrected result is used as input parameters for the cluster dynamics simulations.

3.2. Cluster dynamics model

Cluster dynamics describes the formation and evolution of defects and solute atoms in materials based on the rate-theory method. It is often used to model the irradiation-induced evolution of material over long time-scales. Cluster dynamics is based on a mean-field approach, in which it is assumed that the point-defect production and annihilation take place continuously in time and space, and that all defects are uniformly distributed in the irradiated volume. In this approach, the production, diffusion, and annihilation of defects are modeled by a set of coupled ordinary differential equations that describe the kinetics of the reaction between point defects and other microstructural features. With such description, the microstructure evolution can be simulated up to the time scales of the present irradiation experiment and beyond.

The aim here is to build up a cluster dynamics model for the vacancy-assisted diffusion of Cu atoms and their clustering. Electron irradiation, either from gamma driven Compton scattering or directly from an accelerator, creates isolated FPs and self-interstitial atoms (SIAs). Given the low damage rate, the dominant terms for the defect population evolution are mutual recombination and diffusion towards sinks. The defect populations are described by the following equations:

$$\frac{dC_v}{dt} = R_d(1 - k_{CP}) - k_r C_v C_i - D_v Z_v \rho_d C_v$$

$$\frac{dC_i}{dt} = R_d(1 - k_{CP}) - k_r C_i C_v - D_i Z_i \rho_d C_i \quad (1)$$

where, C_δ (δ = v, i for vacancies and SIAs, respectively) is the defect concentration; R_d is the defect production rate; k_r is the recombination coefficient; D_δ is the defect diffusivity; Z_δ is the capture efficiency by dislocations; ρ_d is the dislocation density; and k_{CP} is the close-pair recombination factor, i.e., the fraction of Frenkel pairs that recombine nearly immediately after the ballistic event and does thus not contribute to the long-range atomic diffusion.

The migration of copper atoms occurs essentially only by the vacancy mechanism [24,25], since the interaction between Cu solutes and self-interstitial defects in iron is repulsive or negligible [26,27]. Di-vacancies or larger clusters are very unlikely to form directly in the damage events given the low energy transfer, and are also very unlikely to form during ageing given the very dilute defect conditions. Interstitial clusters are also very unlikely to form and would have insignificant effect on the Cu diffusion. However, the existence of interstitials can alter the Cu solubility limit and effectively raise the Cu solution energy [28]. The copper diffusivity under irradiation can be estimated as [29]:

$$D_{Cu} = D_{Cu}^{th} \frac{C_v}{C_v^{th}} \quad (2)$$

where, D_{Cu}^{th} and C_v^{th} are the copper diffusivity and vacancy concentration in thermal (non-irradiated) conditions, respectively. The thermal diffusivity of Cu can be written as [29]:

$$D_{Cu}^{th} = D_0 \exp\left(\frac{-E_{Cu}^{act}}{k_B T}\right) \quad (3)$$

where, D_0 is the diffusion prefactor and E_{Cu}^{act} is the copper activation enthalpy by vacancy exchange, given by the sum of vacancy formation enthalpy and effective Cu migration enthalpy. These parameters can be obtained either by fitting on experimental data, or by first-principles calculations.

For dilute alloys such as the ones considered in this work, the nucleation and evolution of Cu clusters is described by the following cluster-dynamics model [30]:

$$\frac{dC_n}{dt} = \beta(n-1)C_{n-1} + \alpha(n+1)C_{n+1} - [\beta(n) + \alpha(n)]C_n (\text{for } n \geq 2) \quad (4)$$

where, $\beta(n)$ and $\alpha(n)$, the growth and shrinkage rates of a cluster of size n, are given by:

$$\beta(n) = 4\pi \left(\frac{3V_{at}}{4\pi} n\right)^{1/3} \frac{D_{Cu} C_{Cu}}{V_{at}} \quad (5)$$

and

$$\alpha(n) = 4\pi\left[\frac{3V_{at}}{4\pi}(n-1)\right]^{1/3}\frac{D_{Cu}C_{Cu}^{lim}}{V_{at}}\exp\left\{\frac{A\sigma}{k_BT}\left[n^{2/3}-(n-1)^{2/3}\right]\right\} \quad (6)$$

The equation controlling the concentration of monomers ($n = 1$) can be written as:

$$\frac{dC_1}{dt} = \sum_{n=2}^{\infty}\alpha(n)C_n - \sum_{n=2}^{\infty}\beta(n)C_n - 2\beta(1)C_1 + \alpha(2)C_2 \quad (7)$$

In the previous equations, $A = (36\pi)^{1/3}V_{at}^{2/3}$, and V_{at} is the atomic volume in the precipitate, assumed to be equal to the bulk atomic volume in Fe. σ is the surface energy of a precipitate, which in case of spherical precipitates is given by:

$$\sigma = 1.08\frac{k_B}{a_0^2}T_c'\left(1-\frac{T}{T_c'}\right), \text{ with } T_c' = \frac{\Omega - TS^{nc}}{2k_B} \quad (8)$$

where, S^{nc} is the non-configurational energy; Ω is the Cu solution energy; C_{Cu} is the total Cu concentration per lattice site; C_{Cu}^{lim} is the Cu solubility limit in Fe and a_0 is the Fe bulk lattice parameter.

With this model, it is possible to obtain the irradiation-induced evolution of the mean cluster radius and number density as a function of time. The numerical parameters implemented in the model are listed in Table 3. Grain boundaries are not considered in this model. The Gear predictor corrector algorithm is utilized as integration technique. For the short-time simulations of electron experiment (7 days), the time step is 10^{-4} s. For the long-time simulations of spent-fuel storage (up to 10^5 years), the time step is 0.5 s at the beginning and 1 s after 5 years. The spent-fuel irradiation condition is the G4 condition (burn-up of 60 GWd per ton of uranium) in Ref. [8] for direct comparison. The total damage over 10^5 years is estimated to be 3.85×10^{-7} dpa.

3.3. Atomistic kinetic Monte Carlo simulations

AKMC is an alternative approach to traditional continuum modeling where the microstructure evolution of a crystal is simulated with a stochastic approach [31]. This method can handle relatively large simulation cells (up to billions of atoms) in three dimensions and is therefore suitable for direct comparison to APT results [2,32,33].

In the present work, AKMC is used to simulate electron irradiation on both alloys with the LAKIMOKA code [34] and the MATEO code [35]. The system evolution is driven by the creation of FPs and the thermal diffusion of vacancies and SIAs, although only the vacancy mechanism is effective for the displacement of Cu atoms, due to the Cu-SIA repulsion [27]. The simulation time increment, delta t, is calculated using the traditional residence-time algorithm [31]

$$\Delta t = \frac{1}{\sum \Gamma_i}, \quad (9)$$

where, Γ_i is the jump frequency and i runs over all possible transitions. The input parameters for the AKMC model are essentially the same as for the cluster dynamics model but the atoms and defects diffuse on an actual lattice instead of as evolving mean concentration fields. Central to the time evolution is the jump frequency Γ, written as

$$\Gamma = \nu \cdot \exp\left(\frac{-E_m}{k_BT}\right), \quad (10)$$

where, ν is the attempt frequency, E_m is the migration barrier for a given transition, k_B is the Boltzmann constant and T is the temperature. The Cu concentration is conservatively set to 0.1 at.% for the model FeCu alloy, and to 0.05 at.% for the cast iron. For each concentration, the results are averaged over 10 independent runs with different random seeds. The particular defect migration barriers encountered throughout the simulation vary depending on the composition of the local atomic environment and are obtained using the standard kinetically resolved activation (KRA) approach [2],

$$E_m = E_m^x + \frac{E_f - E_i}{2}, \quad (11)$$

where, E_m^x is the migration barrier for an atom of species x, E_f and E_i are the final and initial system energies after and before the particular transition. In this way, the local chemical environment is taken into account in an effective manner that has proven robust for dilute systems [31]. The system energies are computed with a pair-interaction cohesive model parameterized on *ab initio* data [36]. The simulations are run in three different supercell sizes. The first one (a) is a $3800a_0 \times 28a_0 \times 28a_0$ cell, with periodic boundary conditions applied on the short directions, and two free absorbing surfaces set on the elongated direction to mimic defect sinks in a bulk lattice. These settings are chosen to reproduce the equivalent sink strength of a dislocation density of 10^{14} m^{-2}. The absorbing surface-to-volume ratio in the simulation cell is equivalent to the ratio of dislocation surface over volume in which the dislocation density is 10^{14} m^{-2}. The dislocation is here regarded as a cylinder with a capture radius of 30 Å. We used LAKIMOKA to perform the calculations in this supercell. The second and third supercell sizes are (b) $340a_0 \times 340a_0 \times 100a_0$ and (c) $340a_0 \times 340a_0 \times 300a_0$. The dislocation lines were added in the simulation cell to model the dislocation density of 10^{14} m^{-2}. We used MATEO to perform the calculations in these supercells. Sizes (a) and (b) are used to simulate the Cu clustering under experimental irradiation condition whereas (c) is used to simulate the Cu clustering under repository condition.

4. Results and discussion

4.1. Experimental results

The Cu distribution in the FeCu model alloy before and after irradiation is shown in Fig. 1. It is challenging to see evidence of Cu clustering with the naked eye, as is usual in the nucleation stage. However, when looking at smaller volumes such as in Fig. 2, small Cu clusters are visible. A statistical analysis was performed to obtain quantitative results. Fig. 3 shows the RDF relative to the bulk-normalized Cu concentration: the high post-irradiation value at short distances is a clear indication of Cu clustering. This result is confirmed by the NNDD analysis reported in Fig. 4, namely by the shift towards shorter distances in the irradiated sample. The obtained cluster number density, using MSM, is 6×10^{23} m^{-3} in the irradiated samples, compared to the value of 0.2×10^{23} m^{-3} in the non-irradiated one. The largest detected cluster after irradiation contained 14 atoms. Hence, considering the APT detection efficiency ($\approx$ 37%), it should correspond to about 38 atoms, or a pure-Cu sphere of roughly 1 nm in diameter. Such size is below the resolution limit of most other microstructure characterization techniques.

Concerning the characterization of the cast-iron samples, only one APT specimen successfully provided sufficient statistical data. In this case, the APT analysis showed no clustering tendencies after irradiation. The obtained Cu distribution map is shown in Fig. 5. The RDF, reported in Fig. 6, seems to oscillate around 1, which also indicates no clustering. However, since the statistical accuracy of this RDF is quite poor, it cannot be considered as fully reliable. It is worth mentioning that no carbon content was detected in this APT specimen, implying that the bulk carbon atoms were most likely segregated to existing graphite nodules, dislocations or grain

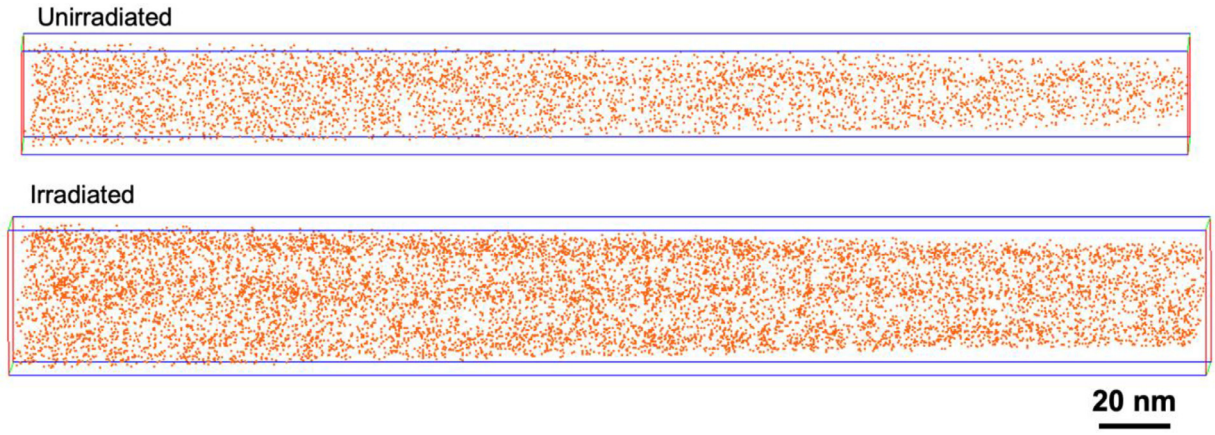

Fig. 1. APT maps of Cu atoms in the non-irradiated and irradiated FeCu model alloy.

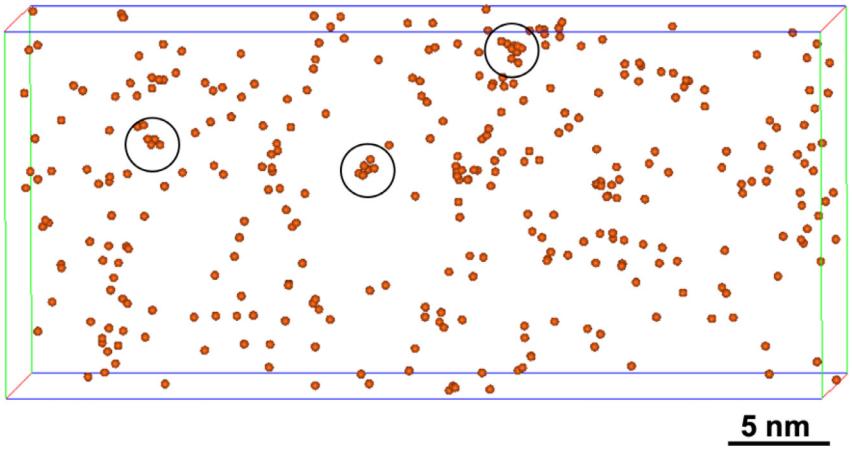

Fig. 2. APT map of Cu atoms in a sub-volume ($18 \times 18 \times 40$ nm^3) of the irradiated FeCu alloy, showing the presence of small clusters.

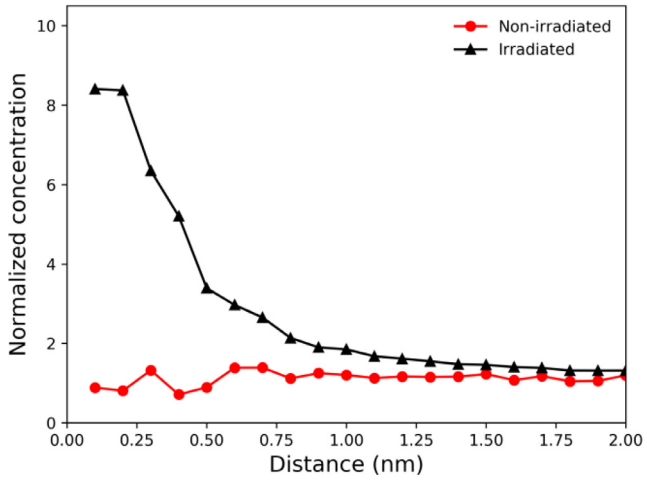

Fig. 3. RDF of Cu-Cu atoms in the FeCu model alloy. The high frequency of short-distanced Cu atoms in the irradiated alloy indicates significant clustering.

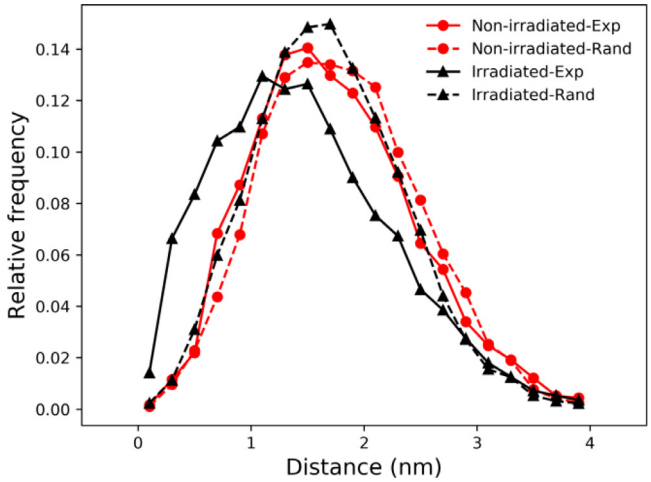

Fig. 4. Nearest-neighbor distance distribution (NNDD) for the irradiated and non-irradiated FeCu model alloy samples. The dashed lines mark the randomized data from each analysis. The irradiated material is characterized by shorter distances between Cu atoms of each pair.

boundaries. The presence of graphite is a likely cause of the low success-rate of the experiments on the cast-iron samples.

4.2. Cluster dynamics parameterization and results

Cluster dynamics is a very parameter-sensitive method. The choice of parameters is vital to yield reasonable results. In this section, we will firstly discuss the choice of the key parameters in our simulation. Then the simulation results will be presented.

4.2.1. . Cluster dynamics parameterization

The close-pair recombination factor k_{CP} is computed with a combined MD-AKMC approach. Firstly, displacement cascades in

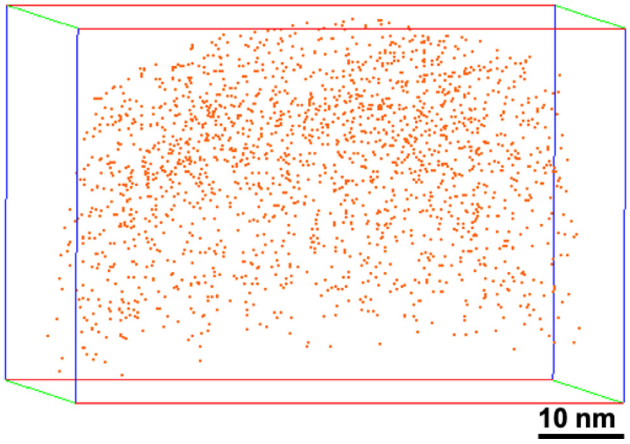

Fig. 5. APT map of Cu atoms in irradiated cast-iron, suggesting a random distribution.

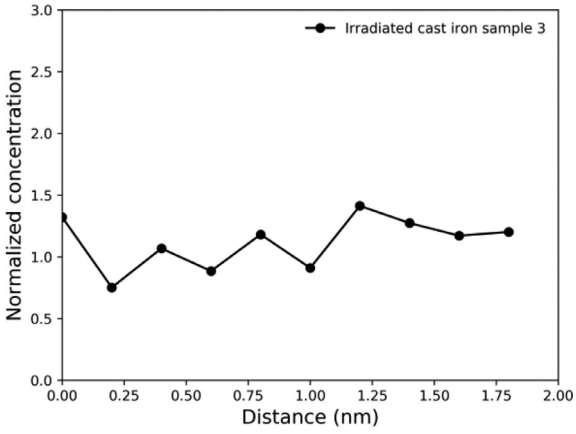

Fig. 6. RDF of Cu-Cu atoms for the irradiated cast iron sample. No clustering is found.

pure iron induced by 2 MeV electrons are simulated using MD up to a few tens of ps, with a time step of 0.1 fs. These MD simulations are based on the well-established Ackland potential [37]. The maximal transferable energy is 232 eV. Therefore, MD simulations are performed by varying the initial knock-out energy from 40 to 232 eV, at 40 eV intervals. Afterwards, a large set of AKMC simulations are performed on the final MD configurations containing at least one stable FP. This is to estimate the fraction of surviving pairs that recombines without performing any long-range migration, thus being unavailable for driving Cu diffusion and clustering. This fraction can be removed from the defect generation rate. As is shown in Fig. 7, the fraction of survived defects in the AKMC simulations ranges from 0.72 to 0.80 depending on the recoil energy. Hence, a reasonable value of $k_{CP} = 0.25$ is set for all calculations.

In cluster dynamics and AKMC simulations, the vacancy formation energy, vacancy migration energy and Cu diffusivity are also key parameters. Table 2 compares two different parameter sets. These parameters can be obtained either classically from interpretation of experiments (parameter set A) which has often been used in literature [8,29] or from DFT calculations (set B) [10,38]. It should be noted that the main differences between parameter set A and set B, which relate to the formation and migration energies, has been extensively studied and seen to be linked to impurity levels in earlier experiments [39]. The difference in values can be readily explained by the carbon-vacancy interaction in iron. To determine which set better reflects the here observed clustering evolution, we compare the simulation results obtained from the

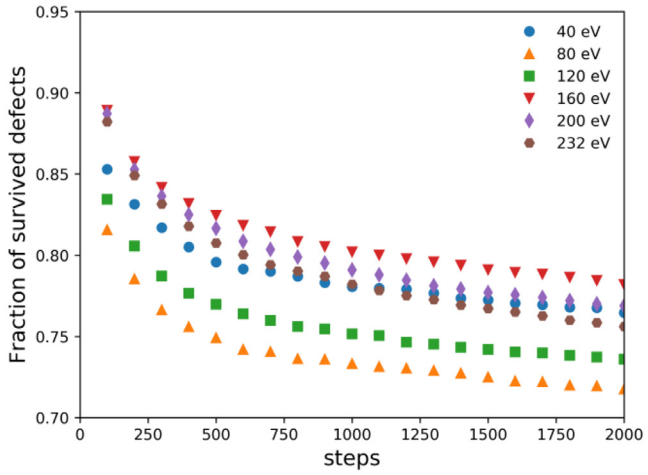

Fig. 7. AKMC-computed fraction of surviving point-defects after short-range migration, for increasing displacement cascade energies. Based on these results, the close-pair recombination factor k_{CP} is set to 0.25.

Table 2
Comparison between two sets of parameters. The set A are the same as Ref. [29], which were derived from experiments. The set B are from DFT calculations. The vacancy formation and migration energies are from Ref. [10] and the Cu diffusivity is from Ref. [38].

	Parameter set A	Parameter set B (DFT)
Vacancy formation energy	1.6 eV	2.1 eV
Vacancy migration energy	1.3 eV	0.7 eV
Cu diffusivity	$0.63\exp(-2.29/k_BT)$ cm^2/s	$0.27\exp(-2.55/k_BT)$ cm^2/s

two parameter sets in Table 2. Fig. 8a shows the simulation results of Cu clustering under experimental irradiation condition for both parameter sets. The Cu solution energy Ω is set close to the experimental reference value. We note that with this choice of parameter, the predicted cluster sizes are significantly larger than the experimentally observed one (which is approximately 0.5 nm in maximal cluster radius). The main reason for the disagreement is that the quantities Ω and S^{nc} provided by Ref. [29] were derived from the experimental copper solubility $C_{Cu}^{lim} = \exp(\frac{S^{nc}}{k_B})\exp(-\frac{\Omega}{k_BT})$ at higher temperature, and then extrapolated down to 140 °C where no direct solubility measurement is available. The low-temperature Cu solution energy Ω provided by Ref. [29] can therefore be considered as affected by large uncertainties. It was thus decided to use the Cu solution energy as a tuning parameter, to reproduce the experimental average cluster radius of 0.5 nm. As is shown in Fig. 8b, such a goal was achieved by setting the Ω to 1.5 times the original value in Ref. [29]. This value, 0.8 eV, coincides with the DFT predicted Cu solution energy [27]. We also note that, in Fig. 8b, both parameter sets give much closer agreement with the here performed experiments. The fully consistent DFT parameters (set B) provide the closer prediction and will thus be used henceforth.

Another parameter of importance, for which an unambiguous experimental is not always available, is the dislocation density. Three different dislocation densities are used in our simulations. The first one is $\rho_d = 10^{12}$ m^{-2} from Ref. [8], which allows for a direct comparison with the results therein. The second dislocation density is $\rho_d = 10^{14}$ m^{-2} from Ref. [40]. This is supposed to be the dislocation density in the FeCu model alloy since the specimens in this work were taken from the same reference project as in Ref. [40]. The third dislocation density is $\rho_d = 5.5 \times 10^{15}$ m^{-2} from Ref. [41]. This dislocation density was chosen for cast iron because the dislocation density in the cast iron samples was assumed to be

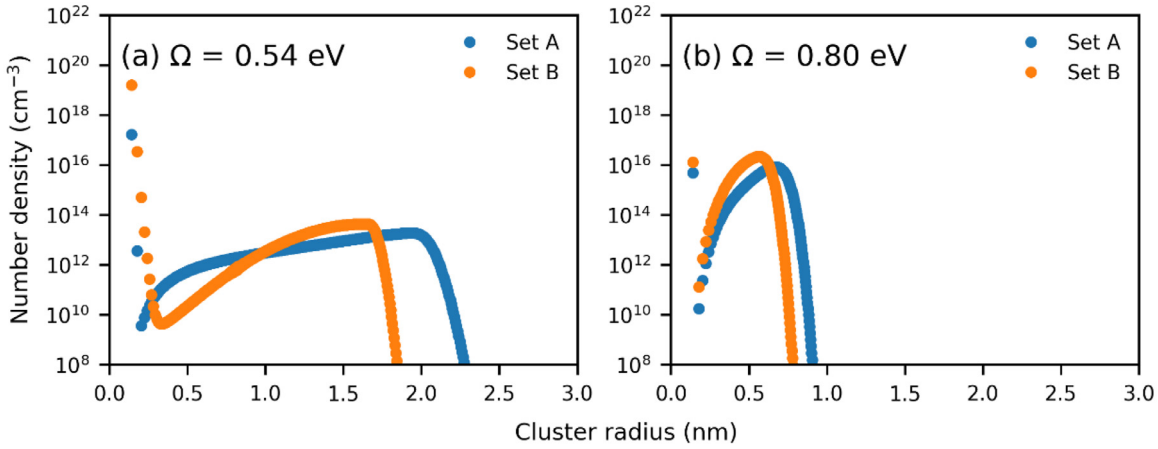

Fig. 8. Comparison between parameter sets; and a comparison between different Cu solution energy. The number densities of clusters are plotted as a function of cluster radius. The dislocation density is set to 10^{14} m^{-2}. The Set A and Set B refer to the parameter sets in Table 2.

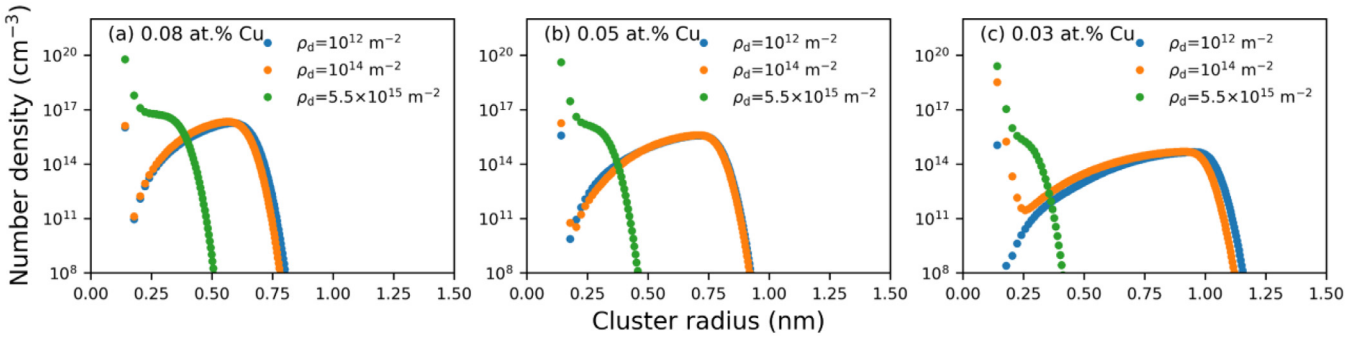

Fig. 9. The simulation results for various Cu concentration and dislocation densities under the experimental irradiation condition and temperature (140 °C) for 7 days. The number densities of clusters are plotted as a function of cluster radius.

Table 3
Parameters used in the cluster dynamics simulations.

Damage dose rate	R_d	$1.81 \cdot 10^{-9}$ dpa/s
Cu solution energy	Ω	0.80 eV [27]
Non-configurational entropy	S^{nc}	$0.866k_B$ [29]
Cu diffusion coefficient	D_{Cu}^{th}	$0.27\exp(-2.55/k_BT)$ cm^2/s [38]
Vacancy formation energy	E_v^f	2.1 eV [10]
Vacancy migration energy	E_v^{mig}	0.7 eV [10]
Vacancy diffusion prefactor	D_v^0	1 cm^2/s [29]
SIA formation energy	E_i^f	4.3 eV [29]
SIA migration energy	E_i^{mig}	0.3 eV [29]
SIA diffusion prefactor	D_i^0	$4 \cdot 10^{-4}$ cm^2/s [29]
Dislocation density	ρ_d	10^{12} m^{-2} [8]
	ρ_d	10^{14} m^{-2} (FeCu alloy)
	ρ_d	$5.5 \cdot 10^{15}$ m^{-2} (Cast iron)

comparable with other cast-iron types. Formation and migration energies of interstitials are the same as in Ref. [29]. Finally, values for the Fe-Cu mixing energy (both the solute segregation energy and the non-configurational entropy S^{nc}) and the point-defect recombination factor are taken from [29].

The parameterization of the cluster dynamics simulation is thus complete. The resulting numerical parameters implemented in the model are listed in Table 3.

4.2.2. Cluster dynamics results

We modelled the clustering of Cu in Fe under the experimental irradiation condition for 143 h at 140 °C. Fig. 9 shows the results with different Cu concentrations for different dislocation densities. It shows that the effect of dislocation density on the clustering is insignificant when the dislocation density is relatively low (ρ_d = 10^{12} m^{-2} to 10^{14} m^{-2}). However, the effect of high dislocation density on the clustering of Cu atoms is significant (ρ_d = 5.5 × 10^{15} m^{-2}). Fig. 9a shows that, for the FeCu model alloy (0.08 at.% Cu), the peak radii of clusters are roughly 0.5–0.6 nm with relatively low dislocation density, which excellently agrees with the experimental observation in Fig. 2. It also supports that our assumed dislocation density of cast iron (10^{12} m^{-2}) is reasonable. At relatively low dislocation density, from Fig. 9a to c, the peak radii of clusters increase to about 1 nm with the decrease of Cu concentration. This increase of cluster size seems to be considerable. Nevertheless, in Fig. 9c, the number density of the clusters is ~10^{14} /cm^3, which is about 2 orders lower than the cluster densities in Fig. 9a. The cluster concentration in 0.03 at.% Cu is thus too low to have significant impact on mechanical properties. Such result indicate that 0.05 at.% Cu is close to the threshold concentration of Cu precipitation under these conditions. This is consistent with the recommended Cu concentration in Ref. [8]. Apart from the Cu concentration, the dislocation density is another key factor that affects the Cu precipitation. For high dislocation density, ρ_d = 5.5 × 10^{15} m^{-2}, essentially no clustering of Cu was obtained at any Cu concentration. Most Cu atoms are in the form of isolated Cu monomers, which means that the precipitation of Cu atoms was hindered by dislocations. This calculation is also consistent with our APT observation on cast iron in Fig. 5. Therefore, we suggest that our assumed dislocation density for cast iron is reasonable. Our simulation results show good agreement with the experimental results for various Cu concentrations and dislocation densities.

Since the cluster dynamics simulation has shown satisfactory agreement with the experimental results, we used the calibrated

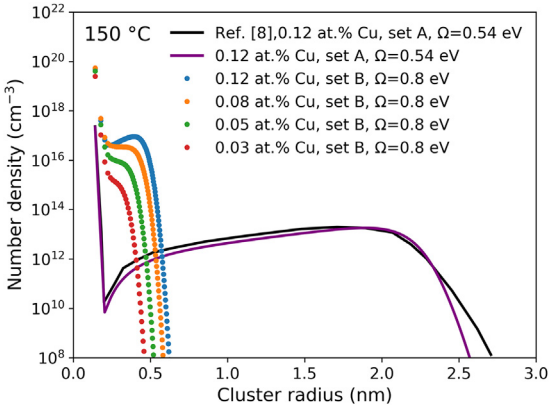

Fig. 10. The simulation results of various Cu concentration under the G4 irradiation condition for 300 years. The number densities of clusters are plotted as a function of cluster radius. The results are compared with Ref. [8].

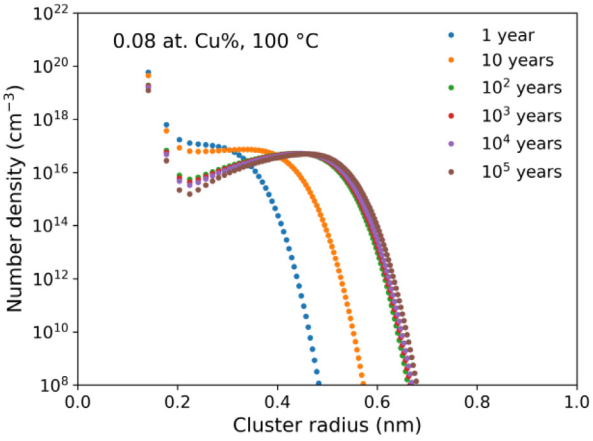

Fig. 11. The simulation results for the time evolution of Cu clustering under G4 irradiation condition. The number densities of clusters are plotted as a function of cluster radius.

model to simulate the Cu clustering after the irradiation of 300 years for various concentrations. In this simulation, to directly compare with Ref. [8], we used the same temperature, 150 °C, dislocation density, $\rho_d = 10^{12}$ m^{-2}, and the same irradiation condition, G4 condition (burn-up of 60 GWd per ton of uranium), as used in the Ref. [8]. For 0.12 at.% Cu, we calculated the Cu clustering after 300 years with the two different parameter sets. The first set is the parameter set A in Table 2 with $\Omega = 0.54$ eV. This is the same parameter set as was used in Ref. [8]. The second set is the DFT parameters used in this work, parameter set B in Table 2 with Cu solution energy, $\Omega = 0.8$ eV. The results are compared with the Ref. [8] in Fig. 10. Our result with the experimental parameters is quite similar to the reference results; the peak cluster radius is roughly 2 nm. However, our result using the parameter set B with $\Omega = 0.8$ eV shows that the peak cluster radius is ~0.4 nm, which significantly differs from the reference result. This disagreement highlights that our method correctly reproduces the results of Ref. [8] and at the same time raises the question as to the validity and applicability of the parameters used in that reference, since the DFT parameters successfully reproduce the evolution seen in our experiments, as demonstrated in Section 4.2.1 and in Fig. 9. Therefore, we argue that our simulation results and consistent DFT parameter set B should be more realistic.

At the beginning of the planned canister deposition, the temperature of the nuclear waste disposal in Sweden is about 100 °C due to self-heating. Over time it will decrease to the temperature of the bedrock, which is near room temperature. The nuclear waste is supposed to be indefinitely stored, but should reach harmless levels of radiotoxicity after about 10^5 years. To make a conservative estimate, for 0.08 at.% Cu, we simulated the Cu clustering after 10^5 years constantly under 100 °C with $\rho_d = 10^{12}$ m^{-2}. Fig. 11 shows the simulated time evolution of the Cu cluster size distribution. It illustrates that most of the Cu clustering happens during the first ~100 years. After that, the evolution of the induced Cu clustering is insignificant. This is because most radioactive fission products with relatively short half-lives would decay and disappear rapidly in ~100 years. After that, the dose rate of long-lived isotopes would be very low and the resulting damage cannot induce significant Cu clustering even after very long time spans. Our simulation results demonstrate that, even with the conservative estimate (relatively high Cu concentration, low dislocation density, constant temperature), the clustering of Cu is essentially insignificant, from a hardening point of view. The peak radii of Cu cluster are ~0.5 nm after 10^5 years. Such small clusters would not cause any significant irradiation-induced hardening in the dilute alloy according to precipitation-driven hardening models [42].

4.3. AKMC results

In order to corroborate the cluster dynamics predictions, the evolution of the Fe-Cu alloys with various Cu concentrations was simulated by AKMC with two different dose rates. The first one is the experimental irradiation dose rate, 10^{-8} dpa/s, up to a total dose of 10^{-3} dpa; the second one is the derived repository dose rate, estimated to about 10^{-17} dpa/s, up to a total dose of

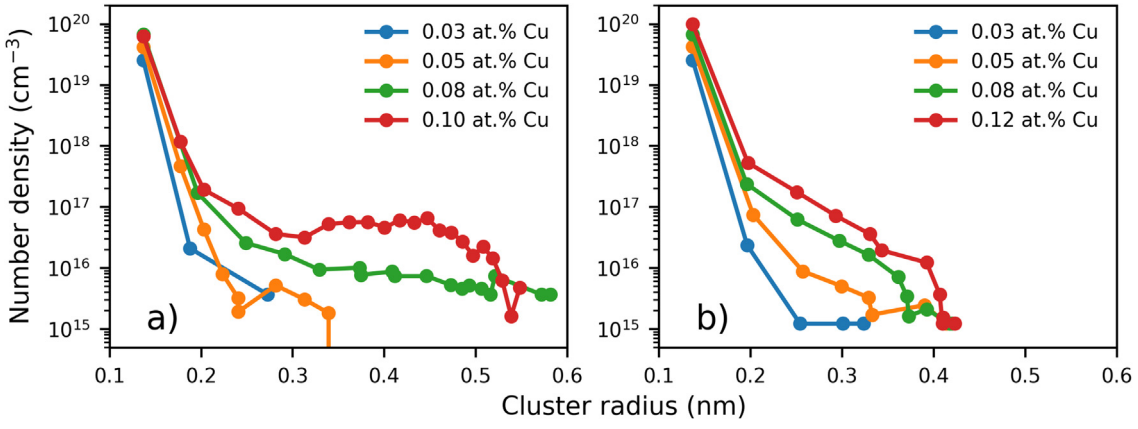

Fig. 12. AKMC Cu cluster distribution as a function of size under (a) the irradiation experiment conditions and (b) the repository conditions.

10^{-4} dpa. The obtained distribution of Cu atoms as a function of cluster size is shown in Fig. 12. Fig. 12a shows that, under the experimental condition, clusters are only formed with relatively high Cu concentration (0.08 and 0.1 at.% Cu). In the case of 0.1 at.% Cu, a peak radius at 0.45 nm is observed (which corresponds to ~30 atoms). This result, obtained without any fitting and based on the *ab initio*-derived cohesive model [36], is in good agreement with the experimental observation and the cluster dynamics results. On the other hand, in the cast iron case (0.03 at.%), some dimers and other small clusters are obtained by AKMC, but at sizes that are surely not distinguishable by APT due to the inherent resolution of the technique. It is thus reasonable to conclude that the simulations in Fig. 12a are in qualitative agreement with the APT observations. Furthermore, there is a satisfactory agreement between the found cluster size distributions using cluster dynamics and AKMC in Fig. 12a.

Fig. 12b shows that, under the repository condition, there is almost no clusters formed even at relatively high Cu concentration up to 10^{-4} dpa. Most Cu atoms are still in the form of isolated monomers after the irradiation. This is because both the dose rate and the total dose are too low to form any considerable amount of Cu clusters. These AKMC results imply that no Cu-precipitation induced hardening is expected in the cast iron insert during the time in which the spent fuel in the canisters is radiotoxic.

5. Conclusions

To study the effect of radiation induced Cu precipitation, which could have consequences for the structural integrity of the cast iron inserts used in the Swedish design for the spent nuclear fuel repository, an electron irradiation experiment has been carried out to simulate accelerated repository conditions. Cast iron and FeCu model alloy samples were irradiated with 2 MeV electrons for one week, and then examined using atom probe tomography. Clusters of about 1 nm in diameter were found in the model alloy, whereas no precipitation was observed in the cast iron.

The experimental damage rate was computed with the electron-scattering Monte Carlo code PIEDMONT, to obtain a more precise estimation with respect to the traditional analytical approximations. This information is then used in cluster dynamics and AKMC models to reproduce the experimental results and build up a reliable framework to simulate the actual repository conditions. In the cluster dynamics calculations, no hardening-induced Cu clustering is predicted for cast iron, whereas in the Fe-Cu model alloy a peak cluster radius of about 0.5–0.6 nm is obtained. Meanwhile, the AKMC simulations parameterized with a well-established *ab initio* cohesive model for RPV steels show a substantial agreement with the experimental results, namely a peak cluster radius of 0.45 nm in the model alloy, and only very small, undetectable clusters in the cast iron model. Finally, the cluster dynamics simulation of a conservative model of the repository conditions for a dilute FeCu alloy did not show any significant clustering, indicating that the spent-fuel canisters materials should be essentially unaffected by Cu-precipitation induced hardening over extremely long timescale.

Declaration of Competing Interest

The authors declare that they have no known competing financial interests or personal relationships that could have appeared to influence the work reported in this paper.

CRediT authorship contribution statement

Qigui Yang: Software, Validation, Formal analysis, Writing – original draft, Writing – review & editing. **Zhongwen Chang:** Software, Validation, Formal analysis, Writing – original draft, Writing – review & editing. **Luca Messina:** Software, Validation, Formal analysis, Writing – original draft, Writing – review & editing. **Nils Sandberg:** Software, Formal analysis, Writing – review & editing. **Nicolas Castin:** Software, Writing – review & editing. **Amine Yousfi:** Investigation, Writing – review & editing. **Elin Toijer:** Validation, Writing – review & editing. **Mattias Thuvander:** Investigation, Writing – review & editing. **Bruno Boizot:** Investigation, Writing – review & editing. **Vincent Metayer:** Investigation. **Dominique Gorse-Pomonti:** Investigation. **Pär Olsson:** Conceptualization, Supervision, Writing – review & editing.

Data availability

Data will be made available on request.

Acknowledgments

This work has been carried out with the financial support of Svensk Kärnbränslehantering AB. Qigui Yang acknowledges the financial support by the China Scholarship Council (No. 201807930008). The computational resources were provided by the Swedish National Infrastructure for Computing (SNIC) and by the CINECA HPC center in Italy. The Authors gratefully thank Christina Lilja and Fredrik Vahlund for their fruitful and helpful discussions. This paper contributes to the Joint Program on Nuclear Materials (JPNM) of the European Energy Research Alliance (EERA).

References

[1] W.J. Phythian, C.A. English, Microstructural evolution in reactor pressure vessel steels, J. Nucl. Mater. 205 (1993) 162–177, doi:10.1016/0022-3115(93)90079-E.
[2] E. Vincent, C.S. Becquart, C. Pareige, P. Pareige, C. Domain, Precipitation of the FeCu system: a critical review of atomic kinetic Monte Carlo simulations, J. Nucl. Mater. 373 (2008) 387–401, doi:10.1016/j.jnucmat.2007.06.016.
[3] N. Castin, M.I. Pascuet, L. Malerba, Modeling the first stages of Cu precipitation in α -Fe using a hybrid atomistic kinetic Monte Carlo approach, J. Chem. Phys. 135 (2011) 064502, doi:10.1063/1.3622045.
[4] N. Castin, M.I. Pascuet, L. Messina, C. Domain, P. Olsson, R.C. Pasianot, L. Malerba, Advanced atomistic models for radiation damage in Fe-based alloys: contributions and future perspectives from artificial neural networks, Comput. Mater. Sci. 148 (2018) 116–130, doi:10.1016/j.commatsci.2018.02.025.
[5] Y. Nagai, Z. Tang, M. Hassegawa, T. Kanai, M. Saneyasu, Irradiation-induced Cu aggregations in Fe: an origin of embrittlement of reactor pressure vessel steels, Phys. Rev. B 63 (2001) 134110, doi:10.1103/PhysRevB.63.134110.
[6] A. Kuramoto, T. Toyama, T. Takeuchi, Y. Nagai, M. Hasegawa, T. Yoshiie, Y. Nishiyama, Post-irradiation annealing behavior of microstructure and hardening of a reactor pressure vessel steel studied by positron annihilation and atom probe tomography, J. Nucl. Mater. 425 (2012) 65–70, doi:10.1016/j.jnucmat.2011.10.019.
[7] M.W. Guinan, Radiation effects in spent nuclear fuel canisters, SKB Technical Report TR-01-32 (2001) skb.se/upload/publications/pdf/TR-01-32.pdf.
[8] L. Brissonneau, A. Barbu, J.L. Bocquet, Radiation effects on the long-term ageing of spent fuel storage containers, Packag. Transp. Storage Secur. Radioact. Mater. 15 (2004) 121–130, doi:10.1179/174650904775295892.
[9] N. Sandberg, P. Korzhavyi, Theoretical study of irradiation induced hardening and embrittlement in spent nuclear fuel holders, relevant for the Swedish long-term storage, SKB Technical Report R-09-15 (2009) skb.se/publication/1930415/R-09-15.pdf.
[10] L. Messina, M. Nastar, T. Garnier, C. Domain, P. Olsson, Exact *ab initio* transport coefficients in bcc Fe – X (X = Cr, Cu, Mn, Ni, P, Si) dilute alloys, Phys. Rev. B 90 (2014) 104203, doi:10.1103/PhysRevB.90.104203.
[11] T. Toyama, F. Takahama, A. Kuramoto, H. Takamizawa, Y. Nozawa, N. Ebisawa, M. Shimodaira, Y. Shimizu, K. Inoue, Y. Nagai, The diffusivity and solubility of copper in ferromagnetic iron at lower temperatures studied by atom probe tomography, Scr. Mater. 83 (2014) 5–8, doi:10.1016/j.scriptamat.2014.03.009.
[12] P. Olsson, C.S. Becquart, C. Domain, *Ab initio* threshold displacement energies in iron, Mater. Res. Lett. 4 (2016) 219–225, doi:10.1080/21663831.2016.1181680.
[13] L. Messina, Monte Carlo Simulation for the Prediction of Gamma-Induced Damage in Metals, KTH Royal Institute of Technology, 2010.
[14] Q. Yang, P. Olsson, Full energy range primary radiation damage model, Phys. Rev. Mater. 5 (2021) 073602, doi:10.1103/PhysRevMaterials.5.073602.
[15] S. Jumel, C. Domain, J. Ruste, J.C. Van Duysen, C. Becquart, A. Legris, P. Pareige, A. Barbu, E. Van Walle, R. Chaouadi, M. Hou, G. Odette, R. Stoller, B. Wirth, Simulation of irradiation effects in reactor pressure vessel steels: the Reactor for Virtual Experiments (REVE) project, J. Test. Eval. 30 (2002) 37, doi:10.1520/JTE12287J.

[16] A. Cerezo, L. Davin, Aspects of the observation of clusters in the 3-dimensional atom probe, Surf. Interface Anal. 39 (2007) 184–188, doi:10.1002/sia.2486.
[17] V. Jaquet, Effet de l'irradiation sur la demixtion des alliages modeles Fe-Cr autour de 15% de chrome, Ph.D. thesis at École Polytechnique, France (2000).
[18] M.J. Norgett, M.T. Robinson, I.M. Torrens, A proposed method of calculating displacement dose rates, Nucl. Eng. Des. 33 (1975) 50–54, doi:10.1016/0029-5493(75)90035-7.
[19] K. Nordlund, S.J. Zinkle, A.E. Sand, F. Granberg, R.S. Averback, R. Stoller, T. Suzudo, L. Malerba, F. Banhart, W.J. Weber, F. Willaime, S.L. Dudarev, D. Simeone, Improving atomic displacement and replacement calculations with physically realistic damage models, Nat. Commun. 9 (2018) 1084, doi:10.1038/s41467-018-03415-5.
[20] F. Maury, M. Biget, P. Vajda, A. Lucasson, P. Lucasson, Anisotropy of defect creation in electron-irradiated iron crystals, Phys. Rev. B 14 (1976) 5303–5313, doi:10.1103/PhysRevB.14.5303.
[21] P.G. Lucasson, R.M. Walker, Production and recovery of electron-induced radiation damage in a number of metals, Phys. Rev. 127 (1962) 485–500, doi:10.1103/PhysRev.127.485.
[22] ASTM E521, Standard practice for investigating the effects of neutron radiation damage, in: Annu. B. ASTM Stand., 2009. 10.1520/E0521-16.
[23] G.H. Kinchin, R.S. Pease, The displacement of atoms in solids by radiation, Rep. Prog. Phys. 18 (1955) 301, doi:10.1088/0034-4885/18/1/301.
[24] A.C. Arokiam, A.V. Barashev, D.J. Bacon, Y.N. Osetsky, Simulation of copper atom diffusion *via* the vacancy mechanism in a dilute Fe-Cu alloy, Phys. Rev. B 71 (2005) 174205, doi:10.1103/PhysRevB.71.174205.
[25] L. Messina, T. Schuler, M. Nastar, M.C. Marinica, P. Olsson, Solute diffusion by self-interstitial defects and radiation-induced segregation in ferritic Fe–X (X=Cr, Cu, Mn, Ni, P, Si) dilute alloys, Acta Mater. 191 (2020) 166–185, doi:10.1016/j.actamat.2020.03.038.
[26] C. Domain, C.S. Becquart, *Ab initio* calculations of defects in Fe and dilute Fe-Cu alloys, Phys. Rev. B 65 (2001) 024103, doi:10.1103/PhysRevB.65.024103.
[27] P. Olsson, T.P.C. Klaver, C. Domain, *Ab initio* study of solute transition-metal interactions with point defects in bcc Fe, Phys. Rev. B 81 (2010) 054102, doi:10.1103/PhysRevB.81.054102.
[28] M. Nastar, L.T. Belkacemi, E. Meslin, M. Loyer-Prost, Thermodynamic model for lattice point defect-mediated semi-coherent precipitation in alloys, Commun. Mater. 2 (2021) 32, doi:10.1038/s43246-021-00136-z.
[29] F. Christien, A. Barbu, Modelling of copper precipitation in iron during thermal aging and irradiation, J. Nucl. Mater. 324 (2004) 90–96, doi:10.1016/j.jnucmat.2003.08.035.
[30] M.H. Mathon, A. Barbu, F. Dunstetter, F. Maury, N. Lorenzelli, C.H. de Novion, Experimental study and modelling of copper precipitation under electron irradiation in dilute FeCu binary alloys, J. Nucl. Mater. 245 (1997) 224–237, doi:10.1016/S0022-3115(97)00010-X.
[31] C.S. Becquart, C. Domain, Introducing chemistry in atomistic kinetic Monte Carlo simulations of Fe alloys under irradiation, Phys. Status Solid 247 (2010) 9–22, doi:10.1002/pssb.200945251.
[32] D. Blavette, E. Cadel, C. Pareige, B. Deconihout, P. Caron, Phase transformation and segregation to lattice defects in Ni-base superalloys, Microsc. Microanal. 13 (2007) 464–483, doi:10.1017/S143192760707078X.
[33] J. Emo, C. Pareige, S. Saillet, C. Domain, P. Pareige, Kinetics of secondary phase precipitation during spinodal decomposition in duplex stainless steels: a kinetic Monte Carlo model – comparison with atom probe tomography experiments, J. Nucl. Mater. 451 (2014) 361–365, doi:10.1016/j.jnucmat.2014.04.025.
[34] C. Domain, C.S. Becquart, L. Malerba, Simulation of radiation damage in Fe alloys: an object kinetic Monte Carlo approach, J. Nucl. Mater. 335 (2004) 121–145, doi:10.1016/j.jnucmat.2004.07.037.
[35] N. Castin, D. Terentyev, A. Bakaev, A. Stankovskiy, G. Bonny, On the equivalence of irradiation conditions on present and future facilities for fusion materials research and qualification: a computational study, J. Nucl. Mater. 562 (2022) 153589, doi:10.1016/j.jnucmat.2022.153589.
[36] R. Ngayam-Happy, C.S. Becquart, C. Domain, First principle-based AKMC modelling of the formation and medium-term evolution of point defect and solute-rich clusters in a neutron irradiated complex Fe–CuMnNiSiP alloy representative of reactor pressure vessel steels, J. Nucl. Mater. 440 (2013) 143–152, doi:10.1016/j.jnucmat.2013.04.081.
[37] G.J. Ackland, M.I. Mendelev, D.J. Srolovitz, S. Han, A.V Barashev, Development of an interatomic potential for phosphorus impurities in α-iron, J. Phys. Condens. Matter. 16 (2004) S2629–S2642, doi:10.1088/0953-8984/16/27/003.
[38] C.D. Versteylen, N.H. van Dijk, M.H.F. Sluiter, First-principles analysis of solute diffusion in dilute bcc Fe-X alloys, Phys. Rev. B 96 (2017) 094105, doi:10.1103/PhysRevB.96.094105.
[39] L. De Schepper, D. Segers, L. Dorikens-Vanpraet, M. Dorikens, G. Knuyt, L.M. Stals, P. Moser, Positron annihilation on pure and carbon-doped α-iron in thermal equilibrium, Phys. Rev. B 27 (1983) 5257–5269, doi:10.1103/PhysRevB.27.5257.
[40] S. Jumel, J.C. Van Duysen, J. Ruste, C. Domain, Interactions between dislocations and irradiation-induced defects in light water reactor pressure vessel steels, J. Nucl. Mater. 346 (2005) 79–97, doi:10.1016/j.jnucmat.2005.04.065.
[41] A.D. Pogrebnjak, O.P. Kul'ment'eva, A.P. Kobzev, Y.N. Tyurin, S.I. Golovenko, A.G. Boiko, Mass transfer and doping during electrolyte-plasma treatment of cast iron, Technol. Phys. Lett. 29 (2003) 312–315, doi:10.1134/1.1573301.
[42] K.C. Russell, L. Brown, A dispersion strengthening model based on differing elastic moduli applied to the iron-copper system, Acta Metall. 20 (1972) 969–974, doi:10.1016/0001-6160(72)90091-0.